11th Australasian Fluid Mechanics Conference
University of Tasmania, Hobart, Australia
14-18 December 1992

PREDICTION OF VORTEX JUNCTION FLOW UPSTREAM OF A SURFACE MOUNTED OBSTACLE

Mark C. THOMPSON and Kerry HOURIGAN

CSIRO Division of Building, Construction & Engineering
PO Box 56, Highett, VIC 3190, AUSTRALIA

ABSTRACT

The structure of the flow near the junction of a surface-mounted obstacle and channel wall is calculated using a three-dimensional multigrid solver for the incompressible Navier-Stokes equations. In particular, the change in flow topology as a function of Reynolds number is investigated.

INTRODUCTION

The flow structure in the vicinity of a cylinder-end wall junction has been investigated experimentally by several authors. Investigation of both laminar and turbulent flows indicates that the structure of upstream flow separation and of the necklace or horseshoe vortex systems is qualitatively similar in both cases. However, the details of the flow behaviour, such as the number of necklace vortices and whether the system is steady, do depend on cylinder geometry and flow conditions. Such flows are of interest for applications such as bridge pier scour.

Gregory and Walker (1951) used smoke to visualise the "horseshoe" vortex system that wraps around the cylinder base. They noted that the strength of the vortex system depends on the Reynolds number and the ratio of cylinder height to boundary layer thickness when this ratio is approximately unity or smaller. Sedney and Kitchens (1975) observed similar behavior. Figure 1 shows schematic representations of the observed behaviour of two configurations observed during their study.

Baker (1979) used smoke to visualise the laminar flow around a cylinder mounted normally to a flat plate. Both steady and unsteady vortex systems were observed. Three different behaviours were identified: (1) steady horseshoe vortex systems with 1,2 or 3 vortices together with the induced counter-rotating vortices attached to the wall between each pair of primary vortices; (2) horseshoe vortex systems which exhibit regular oscillatory motion; and (3) horseshoe vortex systems which exhibit irregular unsteady motion.

Devenport and Simpson (1987) examined the turbulent flow in a boundary layer around the nose of a wing-body junction using surface visualisation and a 3 component laser-doppler system. They found that the there were two distinct regions of flow divided by a line of low streamwise shear: the upstream region characterised by weak backflow, and the downstream region by intense recirculation. The authors suggested that this is consistent with instantaneous large-scale fluctuations in size and position of the junction vortex.

Greco (1990) used hydrogen bubble flow visualisation and hot-film probes to attempt to parameterise the different possible behaviours as a function of cylinder geometry and flow conditions. Five distinct laminar flow regimes were found to exist depending on a complicated relationship between free-stream velocity, cylinder diameter, viscosity and streamwise location.

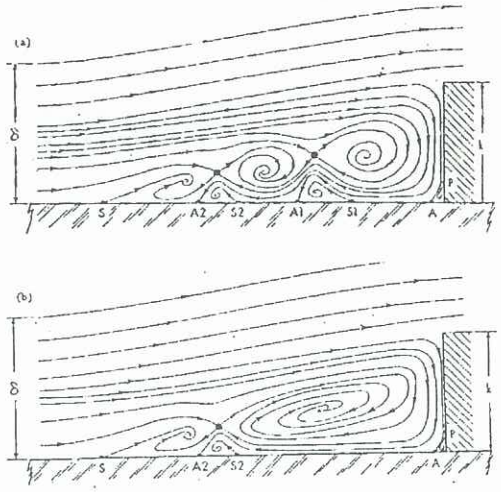

Figure 1: Side-view schematic of streamline pattern in the symmetry plane for flow past a small surface mounted obstable: (a) six-vortex configuration; (b) four vortex configuration. (From Sedney and Kitchens, (1975))

Recently, Deng and Piquet used an 80x45x45 grid to compute the horseshoe vortex structure for a turbulent flow past a wing-body junction. Comparison of calculated skin friction patterns with experimental oil flow visualisations show that the position of the upstream saddle point is well predicted as well as the location of the dividing line separating horseshoe vortex leg flow from the exterior flow. However, the boundary layer thickness is overpredicted, and the streamwise vortices underpredicted most probably due to inadequate resolution away from the aerofoil.

In this paper, the laminar flow past a surface mounted cube in a channel is computed for a range of Reynolds numbers. The mesh is concentrated immediately upstream of the obstacle to achieve the greatest resolution of the vortex (or vortices) near the cube-wall junction.

COMPUTATIONAL METHOD

The incompressible Navier-Stokes equations are discretised using the finite-volume approach. The power-law approximation is used for the convection and diffusion terms (Patankar, 1974)

which uses an approximation to the exponential solution for a one dimensional convection diffusion equation. It behaves like the hybrid scheme except that the transistion from central to upwind differencing is smooth. For some lower Reynolds number runs second-order accuracy is obtained by using the defect correction approach. Unfortunately, the central difference defect correction could not be used for higher Reynolds numbers because the convergence rate of the multigrid iteration scheme is affected adversely unless very fine meshes are used (Thompson and Ferziger, 1989). Details of the particular implementation of the multigrid method to the incompressible Navier-Stokes equations also can be found in that article.

The domain consists of a section of square cross-section channel of height 2 and length 15. A cube of linear dimension 0.5 is placed on the floor of the channel one third of the way along. The inlet and outlet flow is parabolic in both y and z. The flow is assumed to be symmetric in z about the centreplane of the cube so the flow is only computed in one half of the channel. Half of the mesh points in each direction lie in the uniformly spaced submesh ($-1 \le x \le 1, 0 \le y \le 0.5, 0 \le z \le 0.5$). The (half)-cube lies between ($0 \le x \le 0.5, 0 \le y \le 0.5$ and $0 \le z \le 0.25$) inside this submesh. The mesh points are distributed to give good resolution immediately upstream and around the cube. Mesh sizes up to $128 \times 128 \times 64$ are used for most of the calculations with $257 \times 129 \times 65$ used for the computations at Reynolds number 1250. The Reynolds number $Re = UD/\nu$ is defined in terms of the cube width (D) and the maximum inflow velocity (U).

Computational Accuracy

Calculations were performed for Reynolds numbers up to 1250 in steps of 125 and below 125 in steps of 12.5. Figure 2 shows plots of the horizontal velocity along a vertical line 0.6 body widths in front of the obstacle on the centreplane for $Re = 1250$. The line passes approximately through the centre of the primary vortex. Different mesh sizes are compared. There is only a slight difference between the profiles for the finest meshes. At this Reynolds number, the computed velocity field is probably accurate to within a few percent upstream and at the sides of the obstacle. At lower Reynolds numbers the accuracy is better.

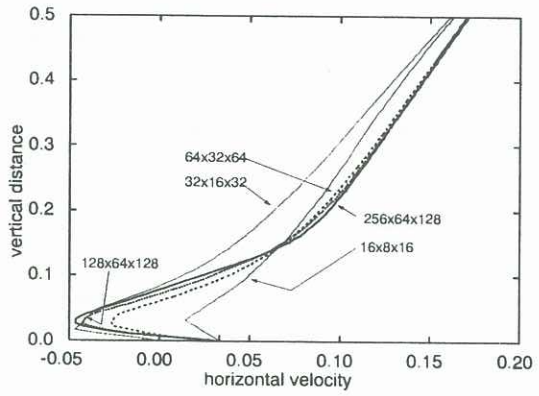

Figure 2: Velocity profiles at $x = 0.6D$ upstream of the cylinder for $Re = 1250$.

RESULTS

Flow Regimes

The topology of the velocity field is a sensitive function of Reynolds number. Figure 3a shows the particle paths on the centreplane upstream of the body for $Re = 100$. In this case there is no upstream vortex. This presumably is because vorticity convected from upstream can be cross-annihiliated by opposite-signed vorticity which is generated by the adverse pressure gradient at the channel floor and then diffuses through the boundary layer. The upstream streamlines converge towards a stable bifurcation line which attaches to the channel floor.

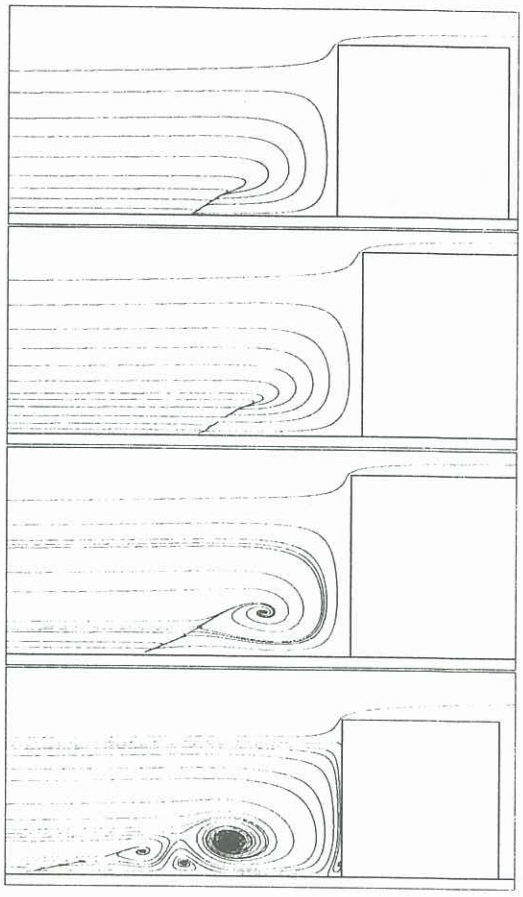

Figure 3: Top to bottom: Streamline pattern on the upstream centreplane for $Re = 100$, 112.5, 250 and 1250, respectively.

At a slightly higher Reynolds number the flow topology changes character. Figure 3b shows the streamline pattern at $Re = 112.5$; here a stable focus is starting to form. This structure represents the beginnings of a horseshoe vortex. The focus is not the only change to the topology; an associated saddle point has also formed. This is the point at which incoming flow either moves up towards the focus or down towards the reattachment point on the channel floor.

At $Re = 250$, (figure 3c), the focus is much stronger but the basic flow topology remains the same. An interesting feature, as pointed out recently by Hung *et al.* (1992), is that the commonly envisaged flow topology, (*e.g., figure 1*), is incorrect in an important detail. The furthest upstream singular point on the floor of the channel is, in fact, a point of attachment and *not* a point of flow separation. This appears to have been originally

noticed by Visbal (1991) who performed numerical simulations of laminar flows over cylinders. This property occurs for all Reynolds numbers considered in this paper. From the smoke flow visualisations (e.g., Thwaites (1960), Baker (1979)), it is not obvious whether the point is an attachment or separation point. However, close examination of the smoke visualisations indicates that the patterns are consistent with flow attachment there. The misinterpretation has probably occurred and been sustained by the belief that flow separation is what one would expect intuitively. The property is difficult to deduce from the flow visualisations alone as evidenced by the large number of authors who have misinterpreted the smoke visualisations and the surface oil patterns.

Between Re = 625 and Re = 750, a secondary horseshoe vortex begins to form together with an opposite-signed vortex situated near the floor of the channel between the primary and secondary horseshoes. The formation of the secondary focus is accompanied by the development of another saddle point. The general topology is depicted in figure 3d which shows the streamline pattern for Re = 1250. The pattern is very similar to that depicted in figure 1b except for the extra saddle point between the secondary horseshoe and the furthest upstream floor attachment point (S of figure 1). Again this is a point of attachment and not separation.

Flow Around the Cylinder and Downstream

Figure 4 shows the flow patterns in planes passing through the vertical centreline of the obstacle. The *streamlines* are calculated by setting the component of velocity normal to the plane to zero. From top to bottom, the diagrams show the flow patterns in the channel centreplane, and at 30, 60 and 90 degrees to the centreplane for Re = 1250. The legs of the primary horseshoe vortex are clearly visible in the last figure and indeed much further downstream. At this Reynolds number the much weaker secondary clockwise horseshoe vortex is absorbed into the primary as the flow is convected downstream and the anticlockwise vortex between the primary and secondary has been pushed away from the obstacle but stays close to the channel floor. At higher Reynolds numbers the secondary clockwise vortex is much stronger and the flow visualisations indicate that the legs of the horseshoe maintain their identity further downstream (Greco, 1990).

Flow Parameters

Figure 5 shows the movement of the primary vortex as the Reynolds number is increased. The vortex moves outwards from the obstacle very slowly as the Reynolds number is increased. The results are broadly consistent with the experimental results of Baker (1979, figure 12).

Figure 6 shows the variation of the distance from the front of the cube (x_L) to the upstream attachment point as a function of Reynolds number. The dependence seems to be approximately linear until the appearance of secondary vortices. At higher Reynolds numbers the dependence is weaker.

DISCUSSION

At very low Reynolds numbers, there is no focus in the separation plane. As it nears the "cylinder", the flow is pushed downwards and back upstream towards a bifurcation line which attaches to the floor of the channel. At a critical Reynolds number, a little above 100 in this case, the flow topology changes

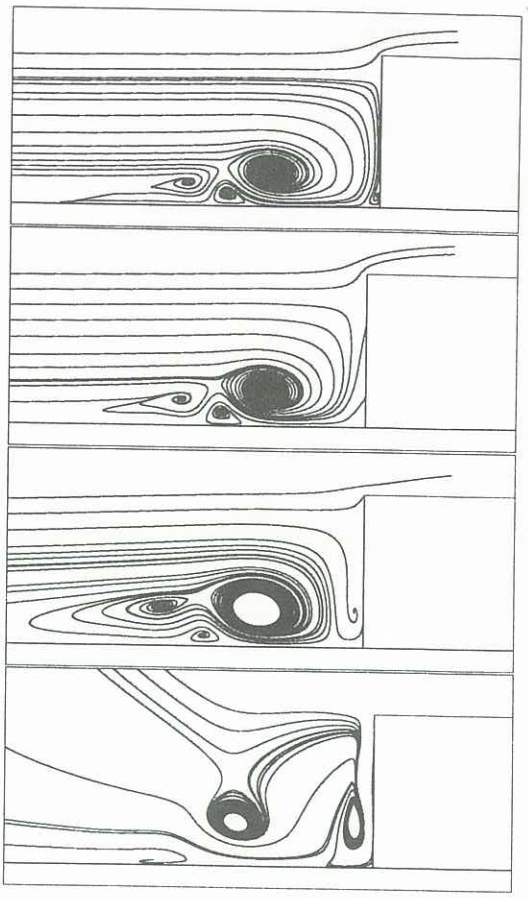

Figure 4: Flow patterns in vertical planes passing through the cube vertical centreline. Top to bottom: 0, 30, 60 and 90 degrees, respectively, measured from the symmetry plane. Re = 1250.

character. The bifurcation line splits, with some incoming fluid forced into a focus, (the beginnings of the primary horseshoe vortex), and the rest moving downwards towards the attachment point. This topology prevails until, at a Reynolds number of approximately 600, the bifurcation line again splits forming a further focus and saddle point. At approximately the same Reynolds number, a counter-rotating vortex forms between the primary and secondary horseshoe vortices.

The dynamics of the situation can be described as follows. Boundary layer vorticity is convected continuously towards the cylinder from upstream at an approximate rate $\frac{1}{2}U^2$, where U is the velocity at the top of the boundary layer (e.g., Morton and Evans-Lopez (1986)). Clearly this vorticity cannot collect at the front of the cylinder without bound. According to the vorticity equation

$$\frac{\partial \omega}{\partial t} + \mathbf{v} \cdot \nabla \omega = \omega \cdot \nabla \mathbf{v} + \nu \nabla^2 \omega,$$

it can be convected, and stretched and reoriented, into the legs of the horseshoe vortex/vortices and it can diffuse and cross-annihilate with opposite-signed vorticity generated (by pressure gradients) at boundaries. The stretching and convection terms do not limit the growth of vorticity. If the flow were inviscid, then Kelvin's theorem would apply and vortex lines travelling from upstream then must wrap around the obstacle to form the horseshoe vortex. Cross-diffusion of opposite-signed vorticity is needed to limit the growth of the horseshoe vortex.

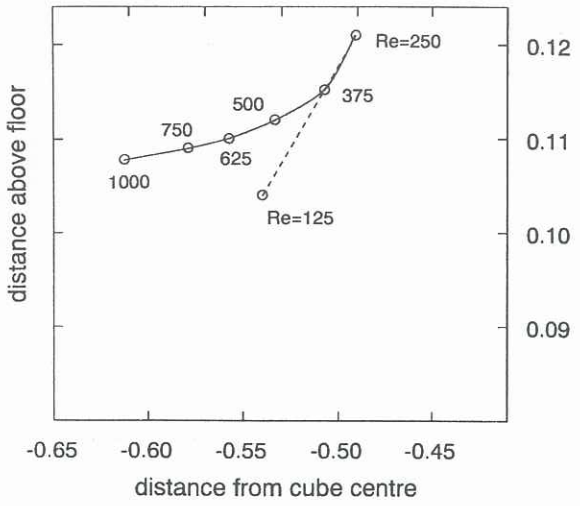

Figure 5: Movement of the primary vortex as a function of Reynolds number.

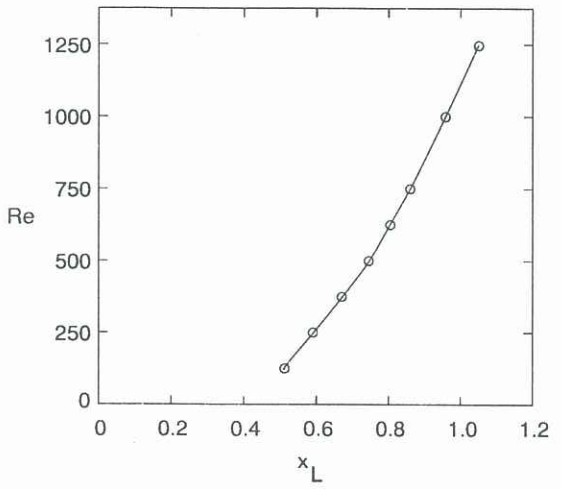

Figure 6: Movement of the upstream attachment point as a function of Reynolds number.

Morton and Evans-Lopez (1986) show that there is generation of opposite-signed vorticity due to pressure gradients at the channel floor at the same rate as it is convected from upstream. At low Reynolds numbers, diffusion from the channel floor is sufficiently rapid to prevent a focus from forming. As the Reynolds number is increased, this is no longer true and the primary vortex begins to form. This process is self-limiting in that the stronger the primary vortex, the stronger the adverse pressure gradient set up beneath it, and the greater the diffusive flux which cross-annihilates the clockwise vorticity. Eventually a Reynolds number is reached at which diffusion can no longer transport the anticlockwise vorticity fast enough through the boundary layer. At this point convection begins to take over. The anticlockwise vorticity generated beneath the primary vortex begins to convect upstream and rolls up into the anticlockwise focus that forms between the primary and secondary clockwise horseshoe vortices.

Figure 7 shows the change in vorticity at the centre of the primary vortex as a function of Reynolds number. At low Reynolds number the strength of the vorticity increases rapidly as vorticity transport and subsequent cross-annihilation is mainly due to diffusion. At higher Reynolds numbers, when the secondary foci begin to form, the wall vorticity is *convected* away from the boundaries into the boundary layer, enhancing mixing and decreasing the rate of increase of primary core vorticity.

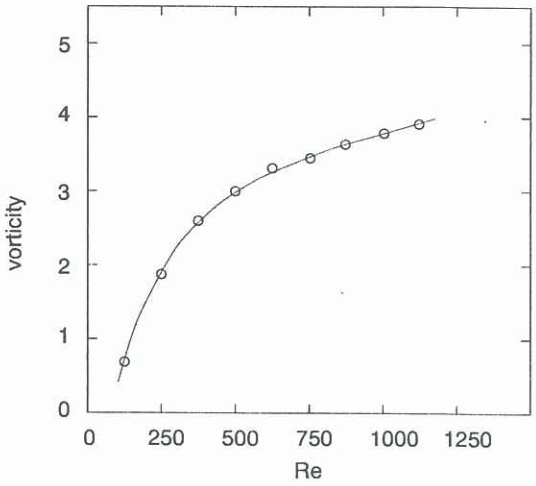

Figure 7: Vorticity at the centre of the primary foci as a function of Reynolds number.

REFERENCES

BAKER, C J (1979) The laminar horseshoe vortex. J. Fluid Mech., 95, 347–367.

DENG, G B and PIQUET, J (1992) Navier-Stokes computation of horseshoe vortex flows, Int. J. Numer. Methods Fluids, 15, 112-124.

DEVENPORT, W J and SIMPSON, R L (1987) The turbulent structure near an appendage-body junction. Report for Aerospace and Ocean Engineering Department, Virginia Polytechnic Institute and State University.

GRECO, J J (1990) The flow structure in the vicinity of a cylinder-flat plate junction: Flow regimes, periodicity and vortex interactions. Masters Thesis, Mechanical Engineering, Lehigh University.

GREGORY, N and WALKER, W C (1951) The effect of transistion of isolated surface excresences in the boundary layer. Rep. Memor. Aero. Res. Council No. 2779, London.

HUNG, C M, SUNG, C H and CHEN, C L (1992) Computation of saddle point of reattachment, AIAA Journal, 30, 1561–1569.

MORTON, B R and EVANS-LOPEZ, J L (1986) Horseshoe vortices and bridge pier erosion. Proc. 9th Australasian Fluid Mech. Conf., Auckland, 256–259.

PATANKAR, S V (1981) Numer. Heat Transfer, 4, 409.

SEDNEY, R and KITCHENS, C W Jr (1975) The structure of three-dimensional separated flows in obstacle boundary-layer interactions. AGARD-CP-168 Report on Flow Separation.

THOMPSON, M C and FERZIGER, J H (1989) An adaptive multigrid technique for the incompressible Navier-Stokes equations, J. Comp. Phys., 82, 94–121.

THWAITES, B (1960) Incompressible aerodynamics. Oxford University Press.

VISBAL, M R (1991) On the structure of laminar juncture flows. AIAA Journal, 29, 1273–1282.